molecular pharmaceutics

Article

pubs.acs.org/molecularpharmaceutics

Rational Development of a Cytotoxic Peptide To Trigger Cell Death

Rebecca J. Boohaker,[†,‡] Ge Zhang,[†,‡] Michael W. Lee,[§] Kathleen N. Nemec,[†] Santimukul Santra,[∥] J. Manuel Perez,[∥] and Annette R. Khaled*[,†]

[†]Burnett School of Biomedical Sciences, College of Medicine, [§]Medical Education, College of Medicine, and [∥]Nanoscience Technology Center, University of Central Florida, Orlando, Florida 32827, United States

Supporting Information

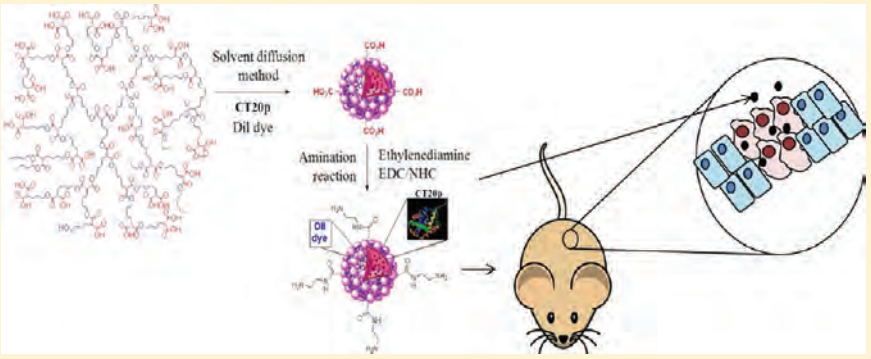

ABSTRACT: Defects in the apoptotic machinery can contribute to tumor formation and resistance to treatment, creating a need to identify new agents that kill cancer cells by alternative mechanisms. To this end, we examined the cytotoxic properties of a novel peptide, CT20p, derived from the C-terminal, alpha-9 helix of Bax, an amphipathic domain with putative membrane binding properties. Like many antimicrobial peptides, CT20p contains clusters of hydrophobic and cationic residues that could enable the peptide to associate with lipid membranes. CT20p caused the release of calcein from mitochondrial-like lipid vesicles without disrupting vesicle integrity and, when expressed as a fusion protein in cells, localized to mitochondria. The amphipathic nature of CT20p allowed it to be encapsulated in polymeric nanoparticles (NPs) that have the capacity to harbor targeting molecules, dyes or drugs. The resulting CT20p-NPs proved an effective killer, *in vitro*, of colon and breast cancer cells, and *in vivo,* using a murine breast cancer tumor model. By introducing CT20p to Bax deficient cells, we demonstrated that the peptide's lethal activity was independent of endogenous Bax. CT20p also caused an increase in the mitochondrial membrane potential that was followed by plasma membrane rupture and cell death, without the characteristic membrane asymmetry associated with apoptosis. We determined that cell death triggered by the CT20p-NPs was minimally dependent on effector caspases and resistant to Bcl-2 overexpression, suggesting that it acts independently of the intrinsic apoptotic death pathway. Furthermore, use of CT20p with the apoptosis-inducing drug, cisplatin, resulted in additive toxicity. These results reveal the novel features of CT20p that allow nanoparticle-mediated delivery to tumors and the potential application in combination therapies to activate multiple death pathways in cancer cells.

KEYWORDS: *necrosis, nanoparticles, metabolism, mitochondria, lipid membranes*

INTRODUCTION

It is generally recognized that cell death can occur through diverse mechanisms, including apoptosis, programmed necrosis, autophagy or mitotic catastrophe. Most studied is the apoptotic pathway that is triggered by extracellular and intracellular cues and is governed by the relative ratios of pro- (i.e.: Bad, Bax, Bim, Bak) to antiapoptotic (i.e.: Bcl-2, Bcl-XL) members of the Bcl-2 family of proteins. Tumors expressing high levels of antiapoptotic proteins, such as Bcl-2, Mcl-1 or Bcl-xl, are often resistant to the effects of chemotherapeutics.[1] This is accomplished, in part, by inhibition of the pro-apoptotic Bcl-2 family members, such as Bax, first identified as a protein that interacts with Bcl-2.[2] A third group of Bcl-2 proteins, identified as the BH3-only proteins such Bid, Bim or Bad, tip the balance between anti- and proapoptotic members and serve as molecular tie breakers favoring cell death.[3] Comparably, less is known about the mechanisms that activate programmed necrosis, autophagy and mitotic catastrophe; however the Bcl-2 family members may play a role in these processes.[4]

To kill cancer cells, conventional chemotherapeutic agents typically rely on an intact apoptotic signaling pathway induced by cellular insults like ionizing radiation (IR), ultraviolet (UV) radiation or reactive oxygen species (ROS) that can cause DNA damage. Resistance to chemotherapeutic agents may result from mutation, duplication or elimination of gene products that

Received: March 29, 2012
Revised: May 11, 2012
Accepted: May 16, 2012
Published: May 16, 2012

are involved in the initiation and/or execution of apoptosis. As an example, DNA alkylating agents become ineffective in tumor cells in which p53 is mutated, resulting in transcriptional loss of Bad and Bax and impairment of the apoptotic program.[5] Due to the prevalence of tumors harboring p53 mutations, recent efforts have focused on directly targeting Bcl-2 family members. Whether acting directly or indirectly on the Bcl-2 proteins, most chemotherapeutic agents cause cytochrome C to be released from mitochondria leading to activation of effector caspases.[6] Thus, given the central role that mitochondria play in life and death, this organelle is a logical target for direct intervention with small molecules or peptides.

Small molecules are stable and have long half-lives. However, *in vivo* efficacy is hard to predict given their extraphysiologic structures that could produce off-target effects.[7] As a result, a number of small molecule cancer therapeutic agents have exhibited significant toxicity when translated for human use.[8] Several small molecule BH3 mimetics, including ABT-737 and navitoclax, are currently being investigated in preclinical and clinical trials.[9,10] Despite their selective affinity for specific antiapoptotic proteins, these compounds appear to be subject to the same constraints that affect other small molecule therapeutics: off-target cytotoxicity.[11]

As an alternative approach to the use of small molecules, anticancer peptide therapy focuses on the development of therapeutic peptides to kill cancer cells.[12] This approach has significant advantages over small molecules, including ease of design and synthesis. A vast knowledge base of normal protein function facilitates the intelligent design of peptides that can specifically target a protein of interest. This study describes the rational development of a cytotoxic peptide that promotes nonapoptotic cell death. Guided by primary sequence similarities of the proapoptotic protein Bax to antimicrobial peptides and the evolutionary relationship of mitochondria to bacteria, we examined the suitability of a peptide modeled after the C-terminus of Bax (CT20p) as a selective pore forming therapeutic. Biophysical studies previously revealed that CT20p could form a pore in mitochondrial-like lipid vesicles, permitting the passage of small molecules (Garg et al. and Tatulian et al., submitted). The purpose of the present study is to determine whether an inherent property of CT20p is the capacity to induce cell death that is nonapoptotic and could result in the direct demise of cancer cells. To introduce CT20p in a vehicle that could be modified for tumor targeting, the peptide was encapsulated in polymeric nanoparticles (NPs). Polymeric NPs are inert particles that have the inherent capacity to incorporate drugs, dyes or tumor-targeting ligands and, thereby, provide an ideal carrier for CT20p. Data presented herein supports the development of CT20p-NPs as a novel cytotoxic agent that can be used alone or in combination therapies for the treatment of cancer.

EXPERIMENTAL SECTION

Cell Lines and CT20p. The Flp-In T-REx-293 cell line (Invitrogen) stably expresses the *lacZ*-Zeocin fusion gene and Tet repressor. The 293 line was maintained in DMEM, 10% fetal bovine serum (FBS) (tetracycline-reduced), 2 mM L-glutamine and 1% penicillin−streptomycin. The HCT-116 $Bax^{-/-}$ and $Bax^{+/+}$ colorectal cancer cell lines[13] (gift from Dr. Bert Vogelstein, Johns Hopkins University) were maintained in McCoy's 5A media, 10% FBS and 1% penicillin−streptomycin. The breast cancer cell lines MCF-7 and MDA-MB-231 (ATCC) were maintained in DMEM, 10% FBS, and 1% penicillin−streptomycin. MCF-7 cells were supplemented with 1% L-glutamine every 15 day. Early passages of all cell lines were frozen as stocks at time of receipt. Cell lines were used at less than 10 passages from stocks. CT20p (Ac-VTIFVAGVL-TASLTI WKKMG-NH2) (Biopeptide Co., Inc.) was commercially synthesized at >98% purity.

Plasmids, Mutagenesis and Transfection. For inducible expression of full-length Bax, we employed the Flp-In T-REx System (Invitrogen) following the manufacturer's protocol. Briefly, PCR-directed mutagenesis of K189/K190 was performed using HA-tagged primer sets (Supplemental Table 1 in the Supporting Information). Bax constructs were amplified from pEGFP-Bax (gift from Dr. Richard Youle, NINDS, NIH), digested with *Eco*RV and cloned into the plasmid pcDNA5/FRT/TO which undergoes DNA recombination at the Flp recombination target (FRT) site when coexpressed with the Flp recombinase pOG44 plasmid. Constructs were confirmed by sequencing; FuGENE transfection reagent (Roche) was used to cotransfect plasmids at a ratio of 9:1. Stable Flp-In T-REx expression cell lines were selected for blasticidin resistance (10 μg/mL), hygromycin resistance (100 μg/mL) and Zeocin sensitivity (200 μg/mL). Bax expression was induced with 1 μg/mL tetracycline. Cells were assayed after 24 h of induction.

To generate the destabilization domain (DD)-tagged Bax C-terminal (CT) constructs (amino acids 173−192) with K189K190 (wild-type) or EE, LL, and RR mutations, primers (Supplemental Table 1 in the Supporting Information) were annealed and ligated into the ProteoTuner vector (Clontech) digested by *Eco*RI and *Bam*HI. Generation of DD-tagged, full-length WT Bax was previously described.[14] The ProteoTuner IRES2 system (Clontech) also had the marker protein GFP downstream to the internal ribosome entry sequence (IRES) and was translated independently of the DD-tagged protein. Cells were transiently transfected using the TransIT-LT1 transfection reagent (Mirus) for 24 h and microscopically assayed for GFP expression. Expression of DD-tagged proteins was induced for 4−5 h by adding 500 nM Shield (Clontech). To generate the EGFP-BAX CT fusion proteins (Supporting Information), primers incorporating the CT (amino acids 173−192) of Bax with mutations targeting K189/K190 (Supplemental Table 1 in the Supporting Information) were used to amplify EGFP from the template pEGFP (Clontech), and the PCR insert was cloned into pcDNA5/FRT/TO as previously above. HCT-116 cells were transiently transfected using the TransIT-LT1 transfection reagent (Mirus) and cells assayed microscopically for EGFP expression up to 12 h later.

MDA-MB-231 cells were transiently transfected with pcDNA-Bcl2 (gift from Dr. Wenqing Li, NCI-Frederick) (or as control pEGFP (Clontech)) using the TransIT-LT1 transfection reagent (Mirus). To assess transfection efficiency, cells were assayed microscopically for EGFP expression. To assess Bcl-2 expression (Supporting Information), cell lysates were immunoblotted as described below.

Mitochondrial Translocation Assay and Immunoblotting. Mitochondrial and cytosolic proteins were isolated using a mitochondrial enrichment kit (Pierce). Western blots were run using 12−15% SDS−PAGE gels and PVDF membranes and probed with the following primary antibodies: 16B12 anti-HA mouse monoclonal (Covance) for HA-tagged Bax; 631073 Anti-DD monoclonal (Clontech) for DD-Bax; N-20 (Santa Cruz), for endogenous Bax, Ab-2 (Fitzgerald) for prohibitin, C20 (MAPK) (Santa Cruz) for p38 MAP kinase, and rabbit

polyclonal for Bcl-2 (Santa Cruz); this was followed by the appropriate secondary antibodies conjugated to horseradish peroxidase (HRP) and visualized with enhanced chemiluminescence kit (Pierce). Molecular weight markers (SeeBlue Plus 2 (Invitrogen)) were used to approximate the position of protein bands in blots.

Live-Cell Confocal Imaging. Images were acquired through a PerkinElmer UltraView spinning disk confocal system, with AxioObserver.Z1 stand (Carl Zeiss), in a humidity- and temperature-controlled chamber (LiveCell) with cells cultured on MatTek plates (MatTek Corporation). Postacquisition snapshots were taken from time-lapse movies at time points indicated in the figures. Time-lapse movies were initiated 2 h after transfection, or expression was induced and images were acquired through 12 h of expression using a Plan-Apochromat 10× objective. For DD-CT20 fusion proteins, cells were incubated with 1 nM MitoTracker Red 580 for 30 min prior to imaging. Time-lapse movies were recorded for up to 12 h using a Plan-Apochromat 63× oil DIC objective.

Visualization of the uptake and effects of the fluorescent dye (DiI)-loaded NPs (prepared as described below) in HCT-116, MCF-7 and MDA-MD-231 cells was observed using a 10× air objective with a numerical aperture of 0.3, using ex/em of 550/587. All cells were loaded with MitoTracker as described above. Visualization of the HCT-116 cell lines was observed using Plan-Apochromat 63× oil objective. MCF-7 and MDA-MB-231 images were captured using Plan-Apochromat 40× oil objective. All time-lapse images were generated in 2D by capturing 6 time points per hour for 24 h of the same field.

Treatment and Detection of Apoptotic Cells and Mitochondrial Membrane Potential by Flow Cytometry. HCT-116, MCF-7 or MDA-MB-231 cells were collected at a final concentration of 1×10^6 cells/mL and assayed using the SYTOX AADvanced dead cell stain solution (Invitrogen). Cells were analyzed using the BD FACSCanto flow cytometer. SYTOX AADvanced was visualized at 488 nm, and emissions were collected at 695 nm. Analysis of data was done using FSC Express software (DeNovo). Membrane asymmetry was assessed using the Violet Ratiometric Membrane Asymmetry Probe/Dead Cell Apoptosis Kit (Invitrogen) according to the manufacturer's protocol.

The cell permeable dye JC-1 (Molecular Probes) was used to qualitatively assess the mitochondrial membrane potential ($\Delta\Psi\mu$). For detection, JC-1 was excited at 488 nm and fluorescence measured at 530 (JC-1 monomers) and 590 (JC-1 aggregates) nm. JC-1 monomers accumulate in the cytosol, while JC-1 aggregates accumulate in the mitochondrial matrix in a manner dependent on the mitochondrial membrane potential. Briefly, MDA-MB-231 cells were seeded in 6 well plates and treated with CT20p or controls as described in the figure legends. JC-1 was used at 5 μg/mL, and cells were incubated with the dye for 15 min in the dark prior to analysis. Cells were analyzed by flow cytometry using the FACSCanto II (BD Biosciences). Data was acquired in the FITC and PE channels for analysis. FCS Express software (DeNovo) was used to analyze data.

To study apoptosis, cells were pretreated with 100 μM pan-caspase inhibitor Z-VAD-fmk (EMD Biosciences) or transiently transfected with Bcl-2 (as described above), then treated with either CT20p-NPs (see below) or cisplatin (CDDP) (gift from Dr. Deborah Altomare, UCF) alone or in combination as indicated in the figure legends. Following treatment, cells were analyzed as described above for cell death and membrane asymmetry.

Synthesis of Polymeric NPs Encapsulating CT20p. CT20p was encapsulated into hyperbranched polymeric (HBPE) NPs following a previously reported method.[15] A fluorescent dye (DiI) was coencapsulated with the peptide. In brief, 1.0 μL of DiI dye (10 μg/μL) and 36 μL of CT20p (0.05 μg/μL) were mixed in 250 μL of a DMSO solution containing the HBPE polymer (12 mg) for a ratio of ~0.15 μg peptide:1 mg nanoparticles. The resulting polymer-DiI/CT20p mixture in DMSO was added to deionized water (2.5 mL) to form the HBPE (CT20p/DiI) NPs. The resulting NPs were purified using a PD-10 column and dialyzed (MWCO 6−8K) against PBS (pH = 7.4). Dynamic light scattering and zeta potential analysis of the nanoparticle reveals a size diameter of 88 ± 2 nm and zeta potential of −54.5 mV.

Synthesis of Aminated Polymeric NPs Encapsulating CT20p. The HBPE NPs (above) contain functional carboxylic groups on their surface that result in a negative charge. To introduce a positively charged surface the nanoparticles were aminated using water-soluble carbodiimide chemistry [EDC, 1-ethyl-3-(3-dimethylamino-propyl) carbodiimide hydrochloride; NHS, *N*-hydroxysuccinimide chemistry], following a previously reported method.[15] Briefly, to a solution of HBPE (CT20p/DiI) NPs (1.0 mmol) in PBS (pH = 7.4), a solution of EDC (10 mmol) and NHS (10 mmol) in MES buffer (pH = 6.0) was added. Afterward, ethylenediamine (10 mmol) in DMSO was added to obtain aminated DiI/CT20p coencapsulation polymeric NPs, which were purified and dialyzed as above. Dynamic light scattering and zeta potential analysis of the nanoparticle reveals a nanoparticle size diameter of 91 ± 3 nm and zeta potential of +10.3 mV. All NPs were stored at 4 °C. A final working concentration of 350 pM was determined by testing the toxicity of 7, 1.4, 0.7 and 0.35 nM on $HCT116^{+/+}$ cells.

Calcein Release Experimental Protocol. Calcein release from artificial membranes was measured on a JASCO 810 spectropolarimeter (Jasco Inc.) with a Peltier water cooled thermostat and a photomultiplier tube mounted at 90° for fluorescence measurements. Large unilamellar vesicles (LUVs) were prepared with the following modifications. Lipids (Avanti Polar Lipids) in chloroform were mixed in the following molar ratios: 52.5% 1-palmitoyl-2-oleyl-*sn*-glycero-3-phosphatidylcholine (POPC), 21% 1-palmitoyl-2-oleyl-*sn*-glycero-3-phosphatidylethanolamine (POPE), 13% bovine liver L-α phosphatidylinositol (PI), 10% cholesterol and 3.5% 1-palmitoyl-2-oleyl-*sn*-glycero-3-phosphatidylglycerol (POPG), in order to mimic the outer mitochondrial membrane. After removing chloroform and desiccating, the dried lipid film was resuspended in 50 mM HEPES, pH 7, supplemented with 110 mM NaCl and 80 mM calcein and extruded with Avanti's miniextruder (Alabaster, Alabama). External calcein was removed by gel filtration through a 1.5 × 50 cm Econo-Column (Bio-Rad) freshly packed with Sephadex 50 (GE Healthcare). CT20p was added at concentrations equivalent to those used with cells in culture. Calcein fluorescence was excited at 495 nm, and emission spectra were recorded between 510 and 550 nm (excitation/emission slits: 10/3 nm). Samples were maintained at 37 °C, and a final measurement was taken at 24 h. Maximum calcein release was obtained by the addition of Triton X-100 (0.1% final concentration) to calcein loaded LUVs without nanoparticles that had been incubated at 37 °C for 24 h after the addition of 10 μL of DMSO. LUV integrity was monitored by

Table 1. Comparison of CT20p with Antimicrobial Peptides and Apoptosis-Inducing Peptides

PEPTIDE	SOURCE	SEQUENCE	% HYD	NET CHARGE	Structure
CT20p	Human	*VITFVAGVLTASLTIW***KK***MG*	60	2	alpha/beta
lactoferricin	Bos taurus	*F***K**C**RR***WQW***R***M***KK***LGAPSITCV***RR***AF*	48	1	beta
Indolicidin	Bos taurus	*ILPW***K***WPWWPW***RR***	53	3	beta
Mellitin	Honey Bee	*GIGAVL***K***VLTTGLPALISWI***KRKR***QQ*	46	5	alpha
Brevinin 1	Frog	*FLPVLAGIAA***K***VVPALFC***K***ITKKC*	66	4	unknown
Ranalexin	Frog	*FLGGLI***K***IVPAMICAVT***KK***C*	65	3	alpha
Cecropin A	Insect	**K***W***K***LF***KK***I***EK***VGQN***R***I***RD***GII***K***AGPAVAVVGQATQIA***K***	45	6	alpha
Dermaseptin B2	Frog	*ALW***K**TML***KK***LGTMALHAG***K***AALGAAA***D***TISQGTQ	54	3	alpha
Magainin 2	Frog	*GIG***K***FLHSA***KK***FG***K***AFVGE***I***MNS*	43	3	alpha
CT20p-REV	n/a	*GM***KK***WTTLSATLVGAVFTIV*	60	2	n/a
KLA peptide	synthetic	***K****LA****K****LA****KK****LA****K****LA****K***	57	6	alpha
Bax a5-a6	Human	***D****GNIFNWGRVVALFYFAS****K****LVL****K****V***P***E****L*/***R***T	52	2	alpha
BIM BH3	Human	*M***R***P***E***IWIAQ***E****L****RR****IG****DE***FNA*	40	0	unknown
BID BH3	Human	***ED***//***R***NIA***R***HLAQVG***D***SM***DR***	40	0	unknown
BAK BH3	Human	*GQVG***R***QLAIIG****DD***INR***	40	0	unknown

Hydrophobic residues are italicized and cationic or anionic residues are in bold and underlined.

light scattering at an excitation wavelength of 500 nm and detected at 90° to the incident light.

***In Vivo* Experiments.** Two to five million MDA-MB-231 cells were harvested from culture and injected subcutaneously into the right flanks of 16 female nude mice (nu/nu, Charles River). After 2−3 weeks, tumor volume and growth were assessed by ultrasound (VisualSonics Vevo 2100). Mice with tumors were injected intratumorally (IT) or intravenously (IV) with unloaded NPs or CT20p-NPs at 4× the concentrations described above. Injections were performed once (IV) or twice (IT) over a 4−15 day period. Mice were observed 0−15 days post-treatments, and tumor area was assessed by 2-dimensional ultrasound by measuring height and width of tumors. Given the size of the standard deviation and the difference in the means between groups of control and CT20p-NP treated mice, at n = 4 for each group, at 80% power the P values were less than 0.05 (StatMate software, Graph Pad). This study was carried out in accordance with the recommendations in the Guide for the Care and Use of Laboratory Animals of the National Institutes of Health. The protocol was approved by the Institutional Animal Care and Use Committee at the University of Central Florida. All efforts were made to minimize suffering.

RESULTS

CT20p Enables Mitochondrial Membrane Binding and Permeabilization. The ability to selectively permeabilize membranes and kill cells is a feature of antimicrobial peptides (AMPs), whose fundamental structure involves clusters of hydrophobic and cationic residues (Table 1). Most peptides with these sequences interact well with the negatively charged prokaryotic lipid membranes but interact poorly with the more zwitterionic eukaryotic plasma membranes.[16] Mitochondria within eukaryotic cells resemble Gram negative bacteria in a number of ways, having a double membrane and circular DNA, and may have arisen through the process of endosymbiosis.[17,18] Hence, AMPs introduced within eukaryotic cells could disrupt mitochondrial membranes, much the way that these damage bacterial membranes, causing mammalian cell death. As example, a synthetic, antimicrobial-like peptide, D-(KLA-KLAK)$_2$, disrupts mitochondria and kills cancer cells when tagged with cell-penetrating peptides.[19−21] Based on this information, we sought to develop a new peptide with the features of AMPs that could be used to induce the selective death of cancer cells. To this end, we examined putative membrane-binding domains from Bax, a death-inducing member of the Bcl-2 family. We found that the C-terminal α9 helix of Bax (basis for CT20p) contained clusters of hydrophobic and cationic residues (Table 1). In fact, the arrangement of hydrophobic and cationic residues of CT20p (or CT20p in reverse (CT20p-REV)) was comparable to a number of AMPs, including those of the brevinin family as well as ranalexin (Table 1). CT20p also shared features with antimicrobial peptides, namely, the double lysines, not found in peptides modeled after the α5-α6 helices of Bax or BH3 domain peptides (Table 1). In fact, based on their sequences, BH3 domain peptides are likely to induce apoptosis by interacting with and blocking the activity of antiapoptotic proteins rather than directly associating with mitochondrial membranes.

To examine the capacity of CT20p to cause cell death by targeting mitochondria, we first examined the involvement of the double lysines in the context of the full-length Bax protein. Mutagenesis of the double lysines in the C-terminus of Bax was performed (results summarized in Supplemental Table 2 in the Supporting Information). Previously we found that constitutive expression of Bax, N-terminal tagged with EGFP as example,

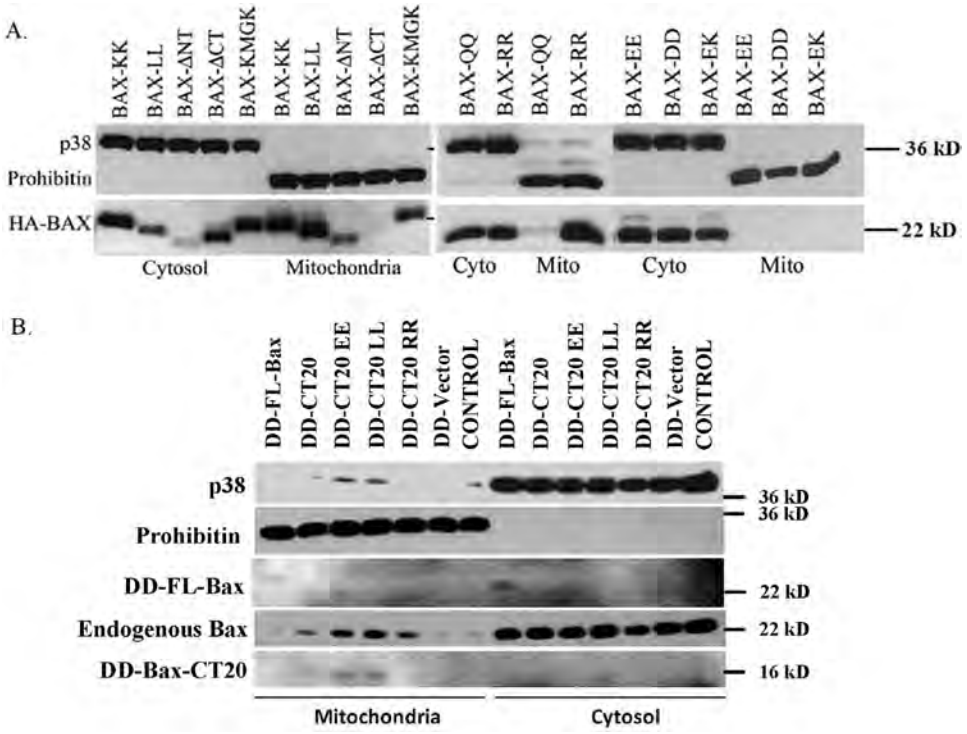

Figure 1. CT20p, based on the C-terminus of Bax, associates with mitochondrial membranes. (A) Mitochondrial translocation of HA-tagged wild type Bax (Bax-KK) and K189/K190 mutants, expressed in 293 cells using the Flp-In T-Rex system, was examined by immunoblot. p38 MAPK and prohibitin were blotted for cytosolic and mitochondrial content, respectively. Data are representative of five independent assays. Images from full-length blots were cropped for concise presentation. (B) The mitochondrial translocation of DD-tagged Bax full-length (FL-Bax) and DD-tagged CT20 peptides, wild-type and EE, LL and RR mutants, was examined in $Bax^{+/+}$ HCT-116 cells by immunoblot. Endogenous Bax was probed with anti-Bax antibody. p38 MAPK and prohibitin indicated cytosolic and mitochondrial content, respectively. DD-fusions were detected with an anti-DD antibody. Controls are cells transfected with empty vector or untransfected. Data are representative of three independent assays. Images from full-length blots were cropped for concise presentation.

induced spontaneous cell death. To avoid this, we inducibly expressed HA-tagged Bax in stably transfected Flp-In T-REx 293 cells. Bax constructs were integrated into the genome at a single FRT (recombination) site, and the levels of Bax expression in these isogenic cell lines did not cause apoptosis. Localization of full-length, wild-type Bax (Bax-KK) was distributed among cytosolic and mitochondrial lysates (Figure 1A) as we and others have previously shown. We found that the N-terminal-deleted Bax (Bax-ΔNT) was localized primarily to mitochondria, while the C-terminal-deleted Bax (Bax-ΔCT) was retained in the cytosol, indicating the importance of the N- and C-terminal domains in the localization of Bax (Figure 1A). Substitution of the double lysines (K189/K190) with negatively charged residues, aspartic acid (D) or glutamic acid (E), resulted in the cytosolic retention of Bax (Bax-DD, Bax-EE) (Figure 1A), whereas substitution of the double lysines with positively charged arginine (R) (Bax-RR) led to mitochondrial localization (Figure 1A). Substitution of the double lysines with a polar amino acid, glutamine (Q) (Bax-QQ), led to less mitochondrial Bax, when compared Bax-KK and Bax-RR (Figures 1A). Substitution of the double lysines with the hydrophobic amino acid leucine (L) (Bax-LL) resulted in mitochondrial association, likely through increased hydrophobicity (Figure 1A). Mutation of one lysine, K189 (Bax-EK), also rendered Bax cytosolic, which was not observed by mutation of K190 (Bax-KMGK) (Figure 1A, Supplemental Table 2 in the Supporting Information). These results confirmed that the double lysines on the C-terminal helix were important for association of the full-length protein with mitochondria.

Next, we determined whether CT20p retained the mitochondrial-binding properties of the full-length protein. To evaluate this, we fused only the CT20p domain to a short destabilization domain (DD) for detection and inducible expression. CT20p fused to DD (DD-CT20) was inducibly expressed in HCT-116 cells. Localization of the fusion peptide was examined postexpression. As control we compared DD-CT20 (KK and EE, LL and RR mutants) to DD-tagged full-length (FL) Bax. Previously, we showed that induced expression of DD-FL Bax did not cause cell death in the absence of apoptotic stimuli.[14] Gene expression was induced for 4 h after previous transfection of cells with DD-FL Bax or DD-CT20 cDNA constructs. Constitutive GFP expression from the bicistronic plasmid was controlled by an IRES element and used to detect transfected cells. As shown in Figure 1B, most of DD-tagged FL Bax was found in cytosolic extracts, and a fraction of DD-FL-Bax was in mitochondria extracts. The small 15−16 kDa band of DD-CT20 or DD-CT20 mutant (EE, LL, and RR (fainter band)) was detected in mitochondrial extracts, indicating that the DD-CT20 was localizing to mitochondria. These results were confirmed by immunofluorescence (Supplemental Figure 1 in the Supporting Information). Expression of DD-CT20 also caused the mitochondrial translocation of a small amount of endogenous Bax (Figure 1B). Additional experiments attaching CT20p to EGFP confirmed the findings that fusion of CT20p to a cytosolic protein could confer membrane association (Supplemental

dx.doi.org/10.1021/mp300167e | Mol. Pharmaceutics 2012, 9, 2080−2093

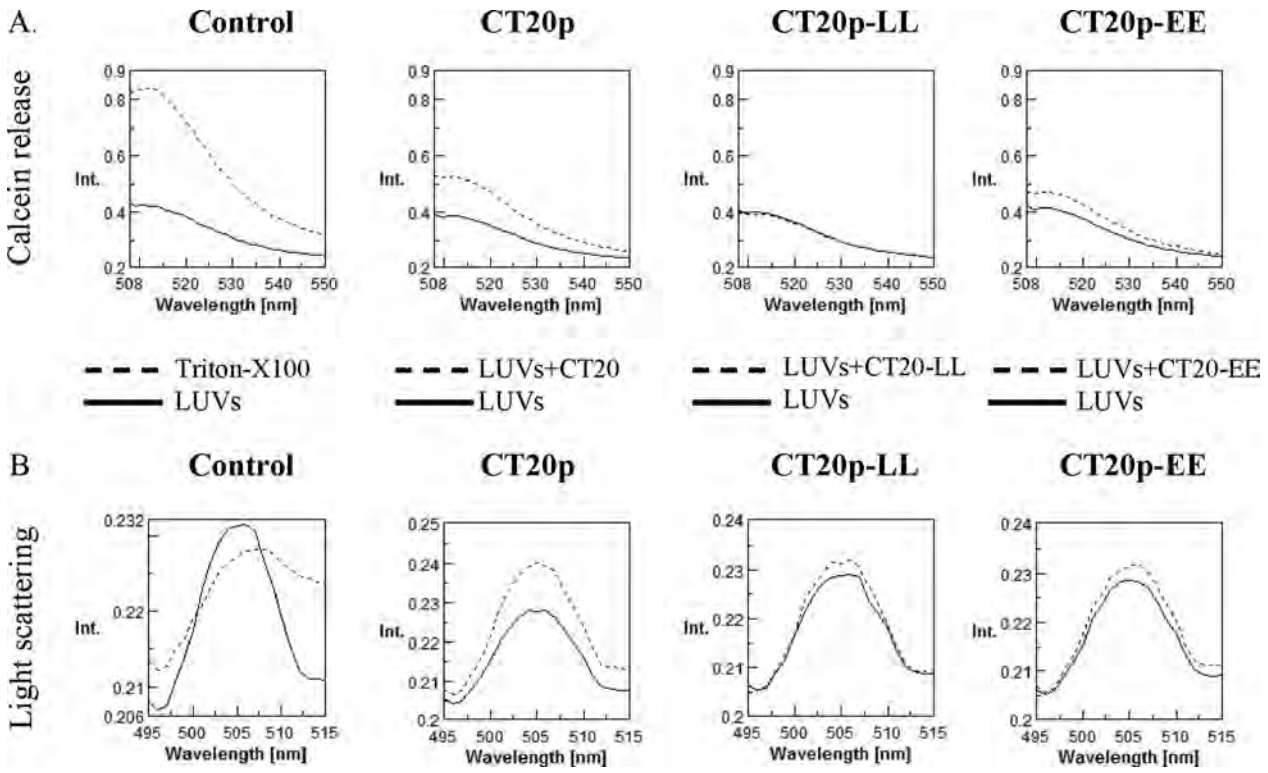

Figure 2. CT20p causes the release of sequestered contents from mitochondrial-like lipid vesicles without loss of membrane integrity. (A) CT20p was commercially synthesized and calcein-loaded mitochondrial-like LUVs prepared. Calcein release from CT20p-treated LUVs was measured as described in the Experimental Section. In the first control figure, dotted lines indicate maximal release of calcein with Triton X-100. In samples treated with CT20p or variants, dotted lines indicate addition of peptide to LUVs and solid lines are LUVs alone in buffer. CT20 is the wild-type peptide, and CT20-LL and CT20-EE are mutations of the double lysines (K189/K190 in the full-length Bax protein). (B) Light scatter analysis of LUVs from panel A. Data are representative of three independent assays.

Figures 2A and 2B in the Supporting Information). It should be noted that, in these experiments, detecting the localization of DD-CT20 or GFP-CT20 proved challenging, even upon a short term of expression, because CT20p expression could cause significant cell death as shown in supplemental figures (Supplemental Figure 2 in the Supporting Information), indicating that its effects upon mitochondria had lethal consequences.

To examine the effect that CT20p could have upon mitochondrial membranes, we directly evaluated its ability to disrupt lipid membranes and cause the release of sequestered contents. LUVs composed of the phospholipids that make up the mitochondrial outer membrane were made as described in the Experimental Section and loaded with calcein. The release of calcein was measured by fluorescence spectrometry. Controls were LUVs alone or LUVs treated with Triton X-100, which caused disruption of lipids and release of calcein. The data in Figure 2A demonstrated that CT20p could insert into mitochondrial-like LUVs and cause the release of calcein (Figure 2A), without disrupting the integrity of the LUVs as was shown by an increase in the light scattering pattern (Figure 2B). A decrease in light scattering is evident when vesicle integrity is lost as seen in the Triton X-100 sample (Figure 2B). The extent of light scattering was determined by the amount of light detected by the fluorescence detector. Because the detector is mounted at a 90° angle from the incident light, any signal detected at the incident wavelength (500 nm) is scattered light. When the double lysines were mutated to leucines (CT20p-LL) or glutamic acids (CT20p-EE), minimal to no release of calcein was detected and LUVs retained their integrity (Figures 2A, 2B). In total, these findings suggest that CT20p can insert into mitochondrial lipid membranes and permeabilize the membranes, perhaps by forming a porelike structure.

Delivery of the CT20p Using Polymeric NPs Kills Cancer Cells. Free peptides in aqueous solutions may not adopt the α-helical conformation needed to penetrate cell membranes. For this reason, modifications, such as chemical stapling,[22] or the addition of membrane-penetrating sequences[23] have been tried by others to deliver free peptides to cells. However, none of these methods can inherently target tumors. To develop a robust intracellular delivery system for CT20p that could combine tumor-targeting ligands as well as conventional drugs, we turned to nanotechnology. As CT20p is soluble and amphipathic in DMSO, it can be encapsulated within the hydrophobic pockets of aliphatic, polymeric NPs. A major advantage of such NPs is their ability to be modified with poly(ethylene glycol) (PEG), reducing nonspecific interactions with proteins, increasing half-life and improving biodistribution and blood circulation time.[24,25] Shown in Figure 3A is the scheme for generating the aliphatic, hyperbranched, polymeric NPs that contain DiI (fluorescent dye) and commercially synthesized CT20p. Two forms of polymeric NPs were made: positively charged, aminated (AM) or negatively charged, carboxylated (COOH) nanoparticles.[15] To verify that the NPs would not release CT20p at neutral pH, calcein loaded liposomes were prepared as above. While CT20p alone resulted in the release of calcein from liposomes (as shown in Figure 2A), CT20p-NPs failed to do so, indicating that the peptide loaded NPs were intact at pH 7 (Supplemental Figure 3 in the

dx.doi.org/10.1021/mp300167e | Mol. Pharmaceutics 2012, 9, 2080−2093

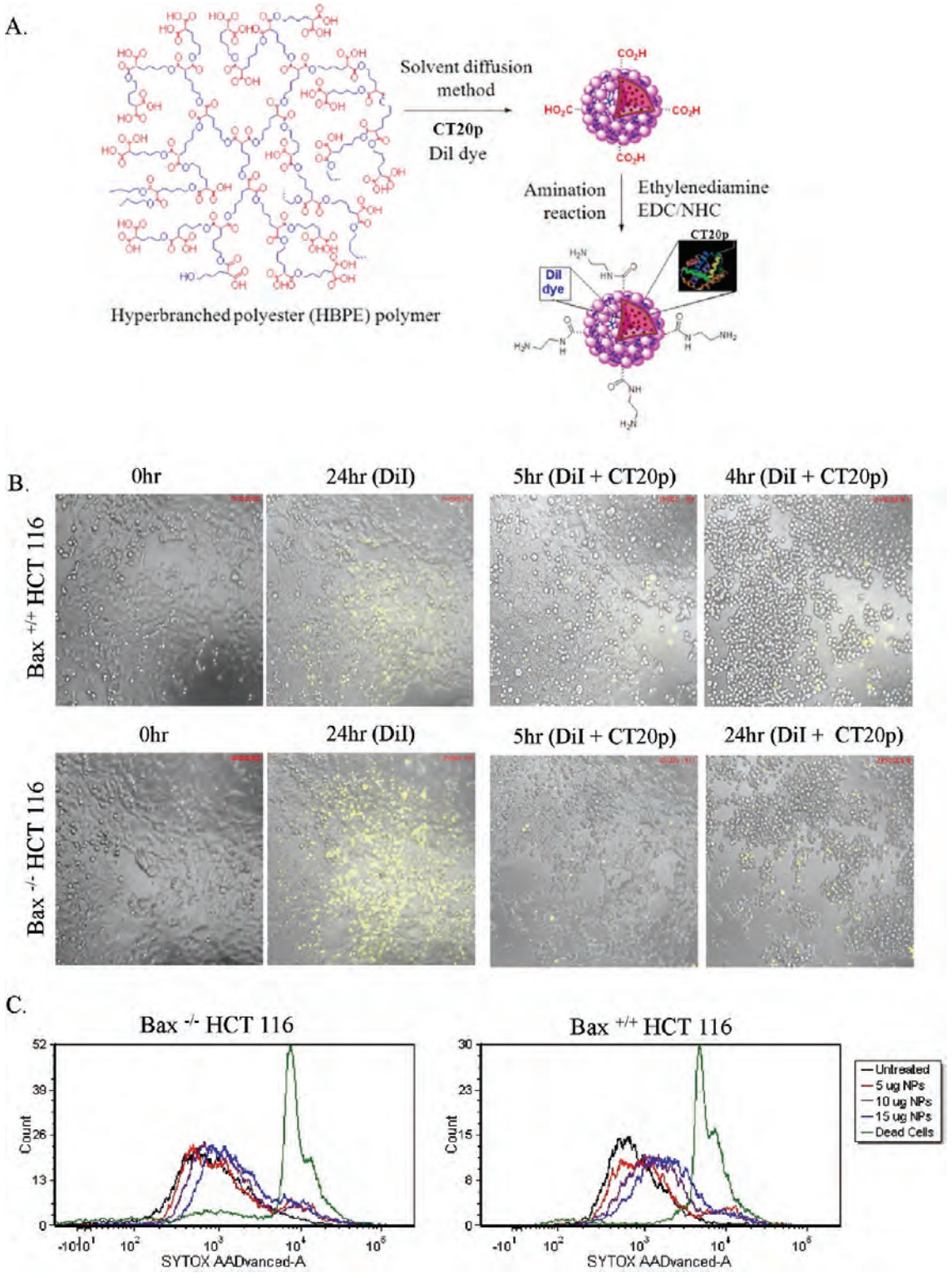

Figure 3. CT20p can be encapsulated in NPs for delivery to cells. (A) Schematic representation of the three-dimensional structure of aliphatic hyperbranched NPs. (B) HCT-116 cells were treated with NPs loaded with DiI or DiI + CT20p (0.07 nM) for 24 h. Time-lapse movies were acquired as described in the Experimental Section using a 10× air objective. For each sample, three different fields of view were acquired. (C) $Bax^{+/+}$ and $Bax^{-/-}$ HCT-116 cells were treated with NPs loaded with DiI at amounts of 5, 10 and 15 μg for 24 h, and cell death was measured using Sytox AAD as described in the Experimental Section. Results or images are representative "snapshots" of three independent experiments.

Supporting Information). This confirmed that cargo is released from NPs only within cells by intracellular esterases or acidic pH,[15] indicating that polymeric NPs are a good vehicle in which to incorporate CT20p for delivery to tumor cells.

Next we examined the uptake of DiI-loaded NPs and their effect upon the viability of HCT-116 cells. The representative experiment in Figure 3B showed that HCT-116 cells take up NPs. Uptake was better for Bax-deficient cells compared to Bax-

dx.doi.org/10.1021/mp300167e | *Mol. Pharmaceutics* 2012, 9, 2080−2093

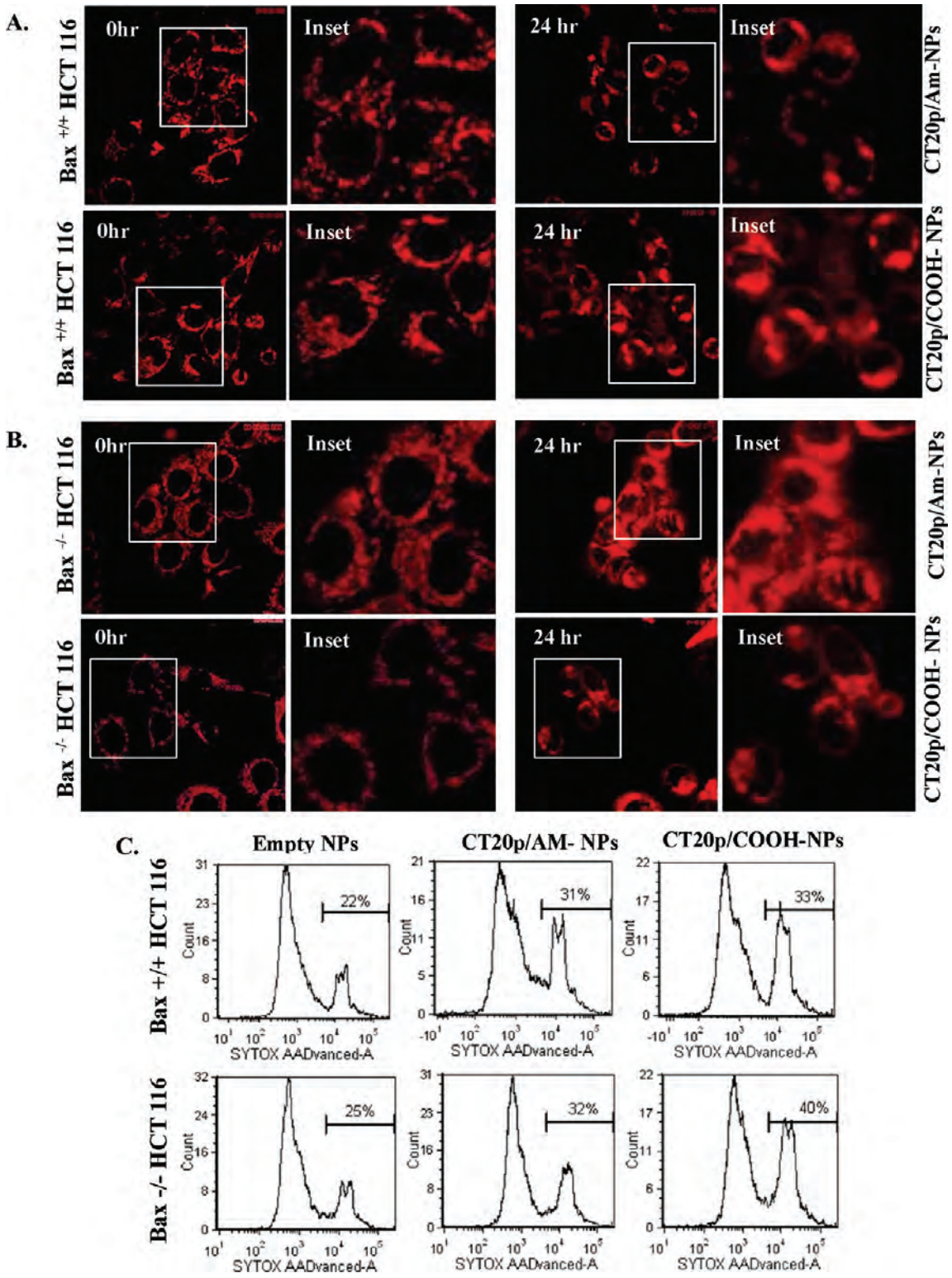

Figure 4. CT20p-NPs kill Bax-containing or Bax-deficient HCT116 cells. (A, B) $Bax^{+/+}$ (A) and $Bax^{-/-}$ (B) HCT-116 cells were treated with AM- or COOH-NPs loaded with CT20p (350 pM) for 24 h. To visualize mitochondria, cells were treated with MitoTracker Red 580 and time-lapse movies were acquired as described in the Experimental Section using a 63× oil objective. For each sample, three different fields of view were acquired. Images are representative "snapshots" of three independent experiments. Insets are digitally enlarged 4-fold. (C) HCT-116 cells were treated with CT20p-NPs (350 pM), and after 3 h, cell death was measured using Sytox AAD as described in the Experimental Section.

containing cells, which in part could be due to their metabolic state since cells lacking Bax tend to be more glycolytic.[14] While the treatment of HCT-116 cells with unloaded NPs did not cause significant cell death (Figure 3B), treatment of HCT-116 cells with CT20p-NPs (700 pM) resulted in observable morphological changes consistent with cell killing (Figure 3B; movie in the Supporting Information). As expected, treatment of cells with free peptide at doses equivalent to that available in

dx.doi.org/10.1021/mp300167e | *Mol. Pharmaceutics* 2012, 9, 2080−2093

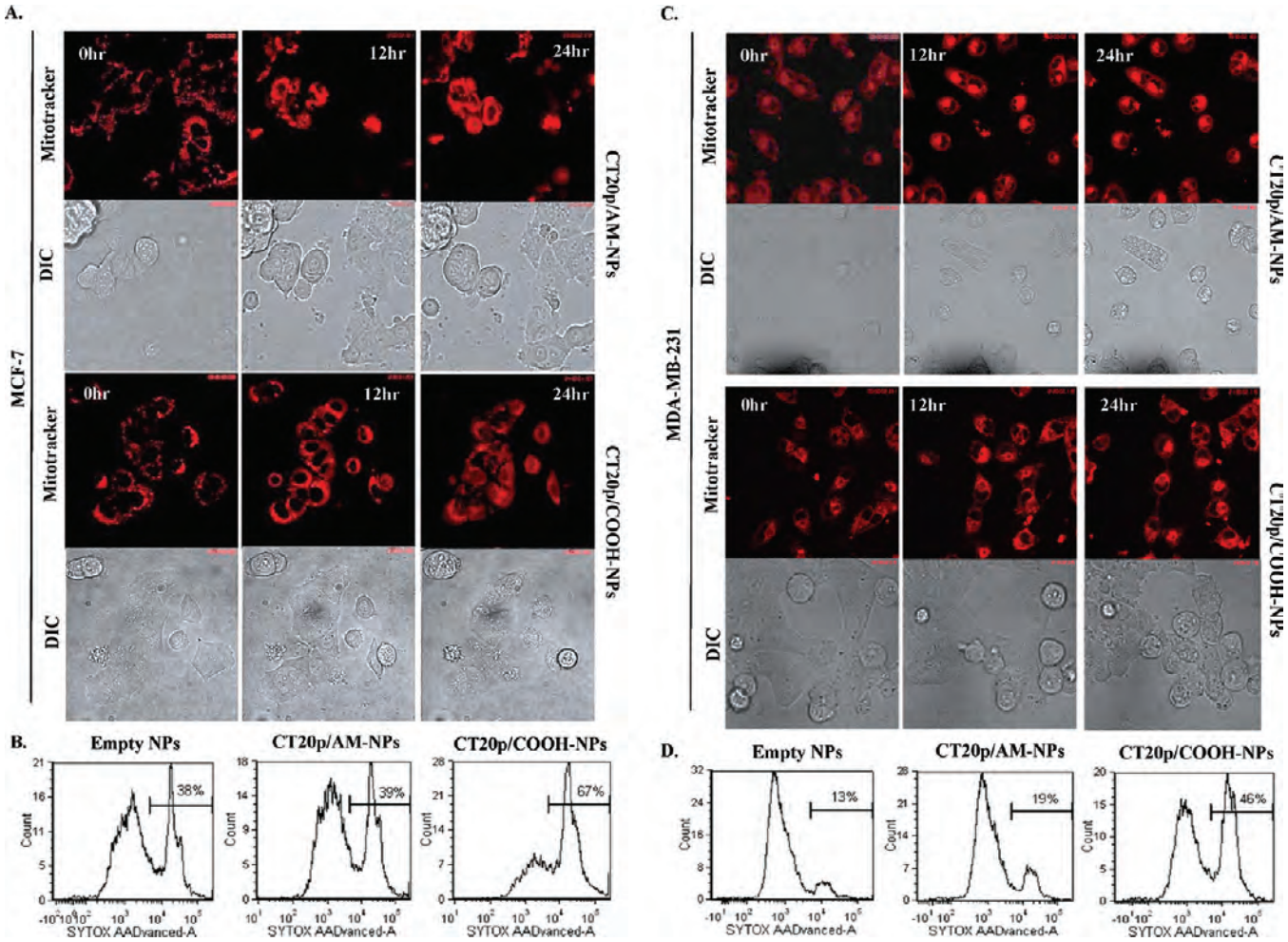

Figure 5. CT20p-NPs kill breast cancer cells. (A, C) MCF-7 (A) or MDA-MB-231 (C) cells were treated with AM- or COOH-NPs loaded with CT20p (350 pM) for 24 h. To visualize mitochondria, cells were treated with MitoTracker Red 580 and time-lapse movies were acquired as described in the Experimental Section using a 40× oil objective. For each sample, three different fields of view were acquired. Images are representative "snapshots" of three independent experiments. (B, D) MCF-7 (B) or MDA-BB-231 (D) cells were treated with CT20p-NPs (350 pM), and after 3 h, cell death was measured using Sytox AAD as described in the Experimental Section.

the NPs as well as 1000-fold greater did not cause cytotoxicity (data not shown). To confirm that NPs alone did not cause death, we used a DNA-binding dye that detects membrane rupture of dead cells (Sytox). In Figure 3C the results show that minimal (in $Bax^{+/+}$ HCT-116 cells) to no (in $Bax^{-/-}$ HCT-116 cells) cell death was detected upon addition of DiI-loaded NPs (5 μg, 10 μg or 15 μg) as compared to positive control (dead cells). From this point on, to minimize off-target effects, all *in vitro* experiments were performed using approximately 350 pM CT20p-NPs.

To visualize the effect of CT20p-NPs on mitochondria, we stained Bax-containing or Bax-deficient HCT-116 cells with MitoTracker and imaged live cells. Figures 4A and 4B are "snapshots" at 0 and 24 h time points revealing changes in cell morphology (see insets) upon CT20p-NP treatment, which include disruption of mitochondria (reduced or diffused MitoTracker staining), cell shrinkage and membrane perturbations, indicative of cell death. Loss of membrane integrity was detected within 3 h of treatment with CT20p-NPs (Figure 4C), more so for the Bax deficient cells that we had shown to more efficiently take up NPs (Figure 3B). While both AM-NPs and COOH-NPs containing CT20p initiated cell death (Figure 4B,C), the COOH-NPs were more effective. Further, these results (Figure 3B and Supplemental Figure 2 in the Supporting Information) with Bax-deficient cells indicated that the death-inducing activity of CT20p was independent of endogenous Bax.

Next, we determined whether CT20p was cytotoxic to the breast cancer cell lines MCF-7 and MDA-MB-231. In Figure 5A, we observed morphological changes such as diffused mitotracker staining and cell shrinkage in MCF-7 cells treated with AM- or COOH-NPs containing CT20p, with COOH-NPs being the more effective. Most MCF-7 cells died within 24 h, while loss of membrane integrity was detected by 3 h of treatment (Figure 5B). In Figure 5C, the live-cell imaging experiment revealed vacuolization and cell shrinkage of MDA-MB-231 cells treated with CT20p-NPs (movie in the Supporting Information). Within 3 h, increased membrane rupture was detected in MDA-MB-231 cells treated with COOH-NPs loaded with CT20p (Figure 5D). Because the cytotoxic effect of the CT20p was more pronounced for the breast cancer cells (Figure 5) compared to HCT116 (especially the Bax-containing HCT116 (Figure 4)), it remains possible that the CT20p-NP compound could be a potent inducer of death in metabolically active cells. These results show that CT20p, once introduced into cancer cells, can rapidly trigger

dx.doi.org/10.1021/mp300167e | *Mol. Pharmaceutics* 2012, 9, 2080−2093

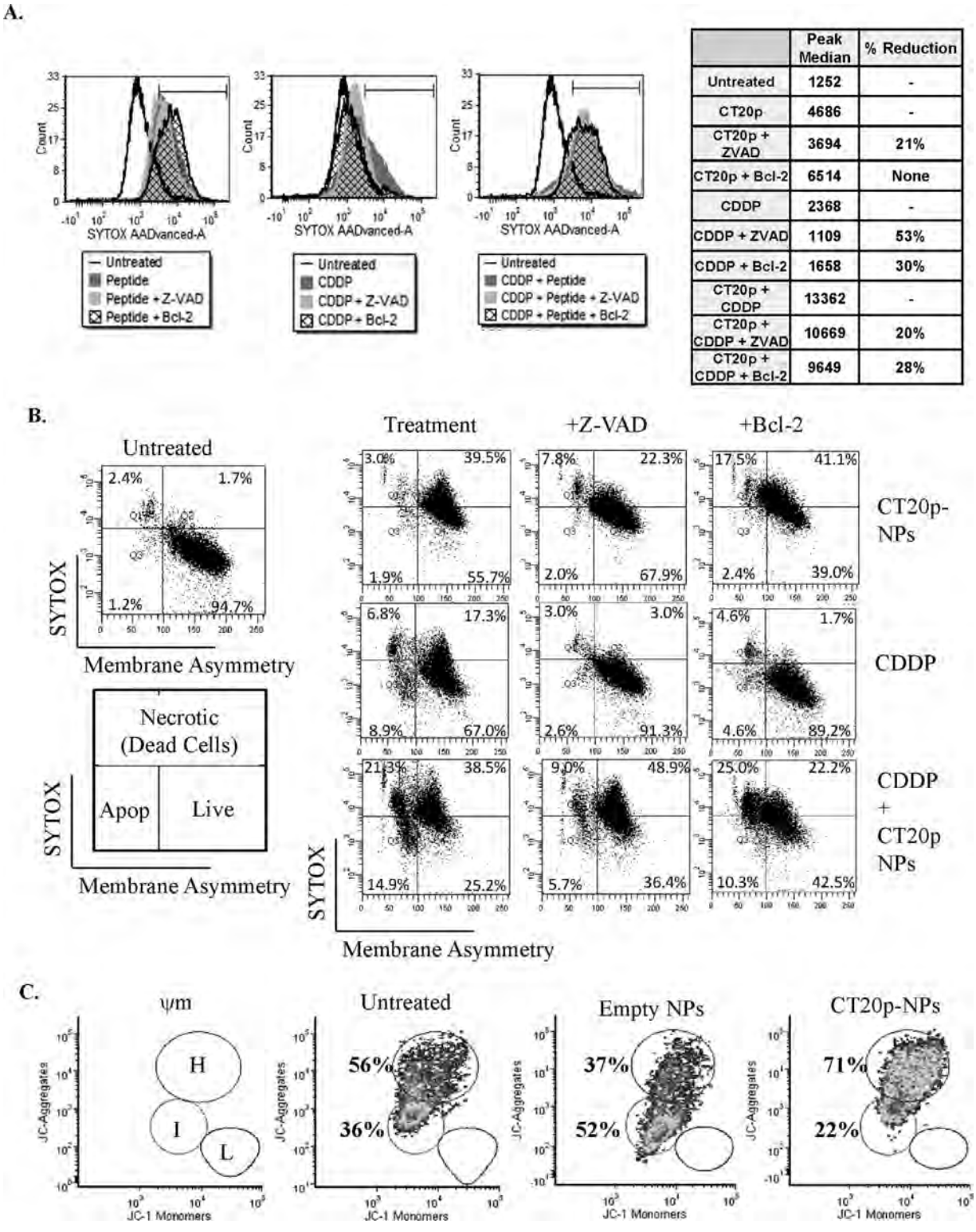

	Peak Median	% Reduction
Untreated	1252	-
CT20p	4686	-
CT20p + ZVAD	3694	21%
CT20p + Bcl-2	6514	None
CDDP	2368	-
CDDP + ZVAD	1109	53%
CDDP + Bcl-2	1658	30%
CT20p + CDDP	13362	-
CT20p + CDDP + ZVAD	10669	20%
CT20p + CDDP + Bcl-2	9649	28%

Figure 6. Mechanism of cancer cell death mediated by CT20p is nonapoptotic. (A) MDA-MB-231 cells were cultured with COOH-NPs, encapsulated with CT20p (350 pM), and treated with ZVAD-Fmk and/or CDDP as described in the Experimental Section. Cells were also transiently transfected with Bcl-2. Cell death was assayed with Sytox AAD. Table shows median peak values for each sample displayed in histograms. (B) MDA-MB-231 cells were treated as described in panel A, and membrane asymmetry was measured with a violet ratiometric probe. Dot blots show a combination of results from Sytox (cell death) and changes in membrane symmetry. (C) Cells treated as described above were stained with JC-1 as described in the Experimental Section to measure mitochondrial membrane potential changes. Dependent on the mitochondrial membrane potential, JC-1 aggregates accumulate in the mitochondrial matrix, while JC-1 monomers are cytosolic. A measurement of JC-1 aggregates to monomers indicates mitochondria with high (H), intermediate (I) or low (L) membrane potential. Data from a 6 h treatment time point is shown. Results shown are representative of at least three independent experiments.

dx.doi.org/10.1021/mp300167e | *Mol. Pharmaceutics* 2012, 9, 2080−2093

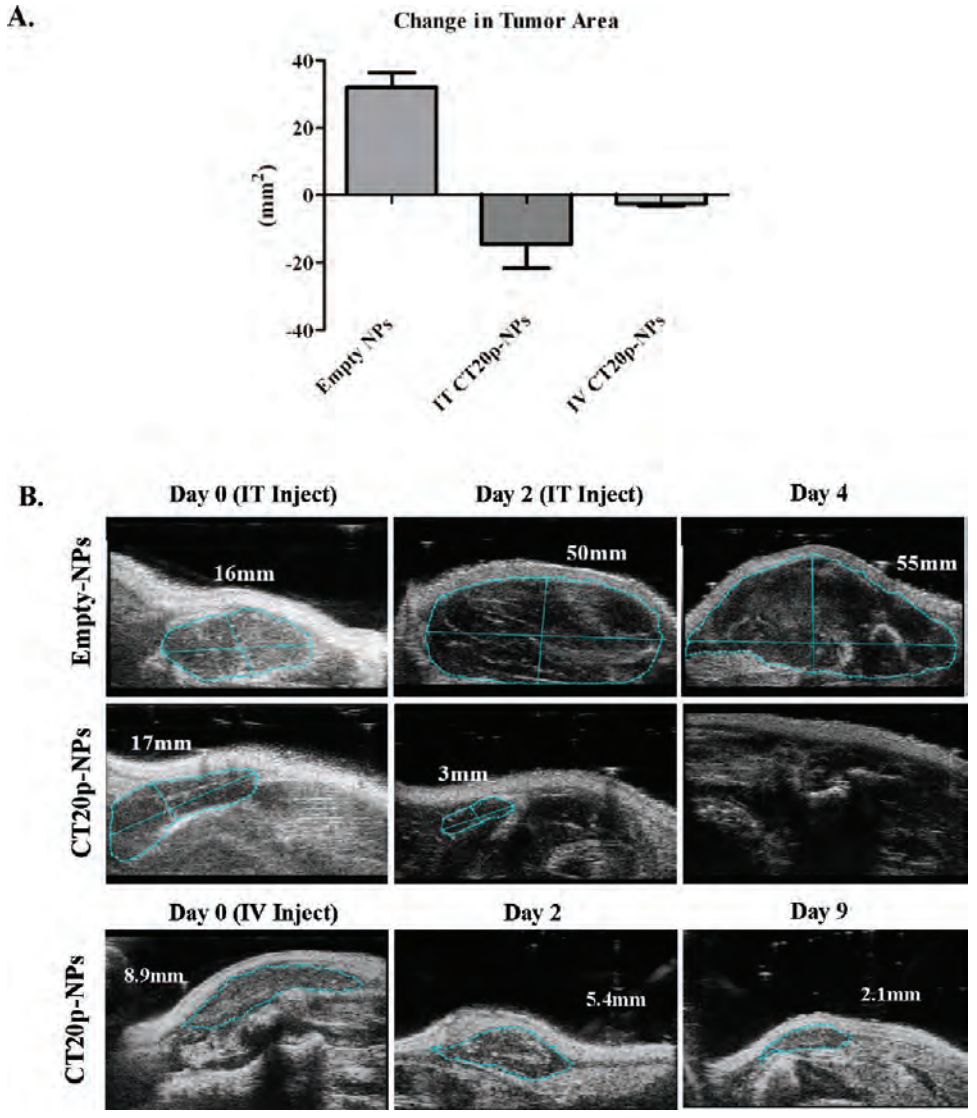

Figure 7. CT20p causes regression of tumors when delivered intratumorally or systemically. (A) MDA-MB-231 cells were implanted in nude mice and changes in tumor area (length × width) assessed by two-dimensional ultrasound as described in the Experimental Section. Mice were treated with either two intratumoral (IT) injections or one intravenous (IV) injection of unloaded NPs (control) or CT20p-NPs. Graph is representative of at least 4 mice per group. (B) Figures are representative ultrasound images of tumor regression induced by treatment with unloaded or CT20p loaded NPs.

cell death, detectable by pronounced morphological changes. Because of these results, subsequent experiments were performed using COOH-NPs to encapsulate CT20p.

The Death-Inducing Activity of CT20p Is Independent of Caspases and Resistant to Bcl-2, Causing Tumor Regression. To investigate whether the mechanism by which CT20p induced cell death involved apoptosis through the intrinsic mitochondrial pathway, we treated MDA-MB-231 cells with CT20p-NPs as described in Figure 5, either adding a caspase inhibitor or overexpressing Bcl-2. Cell death was measured by the uptake of Sytox, an indicator of membrane rupture. As shown in the representative experiment in Figure 6A, CT20p-NPs caused loss of membrane integrity, seen as an increase in Sytox staining, which was minimally impaired by caspase inhibition with Z-VAD-FMK. In contrast, treatment of MDA-MB-231 cells with cisplatin (CDDP) induced less cell death detectable by Sytox but was inhibited over 50% by ZVAD-FMK. These results suggested that the mechanism induced by CT20p could be different from that induced by CDDP, and was largely independent of the effector caspases inhibited by Z-VAD-FMK. We next overexpressed Bcl-2 and found that it did not impair the death activity of CT20p. Overexpression of Bcl-2 did, however, inhibit the effects of CDDP treatment (Figure 6A). Combination of CDDP followed by treatment with CT20p-NPs proved to be the most effective in inducing cytotoxicity that was not significantly inhibited by Z-VAD-FMK or Bcl-2 (Figure 6A). We confirmed that transfected cells were expressing Bcl-2 by immunoblotting lysates prepared from cells (Supplemental Figure 4 in the Supporting Information).

While Sytox is good indicator of cell death, it only reveals whether membrane rupture had occurred. To determine whether CT20p could induce apoptotic cell death, we measured membrane asymmetry caused by flipping of phospholipids in the plasma membrane using a violet ratiometric probe. In Figure 6B, dot blots show the comparison of loss of membrane integrity to changes in membrane symmetry in MDA-MB-231 cells treated with CT20p-NPs

dx.doi.org/10.1021/mp300167e | *Mol. Pharmaceutics* 2012, 9, 2080−2093

and/or CDDP. We found that treatment with CT20p-NPs resulted in uptake of the DNA-binding dye (as shown in Figure 6A), indicating membrane disturbance, but did not promote changes in membrane asymmetry typical of apoptosis. Death induced by CT20p-NPs was slightly affected by caspase inhibition (39.5% reduced to 22% Sytox-positive) but did not approach untreated conditions (1.7% Sytox-positive). Overexpression of Bcl-2 did not block the death-inducing activity of CT20p-NPs (41% Sytox-positive). In contrast, CDDP induced alterations in the membrane asymmetry (~9%) detectable by the violet ratiometric probe that was inhibited by Z-VAD-FMK (2.6%) or Bcl-2 (4.6%) (Figure 6B). The combination treatment of CDDP followed by CT20p-NPs was effective with increased numbers of cells staining positive for both membrane asymmetry and Sytox uptake (~60% combined Sytox-positive). Caspase inhibition or Bcl-2 overexpression minimally affected these results (~58% and ~47% combined Sytox-positive, respectively) (Figure 6B). These findings are suggestive that CT20p could engage a death mechanism distinct from that of CDDP that does not principally involve the intrinsic apoptotic pathway, since death induced was largely independent of ZVAD-FMK inhibited-caspases and resistant to Bcl-2 overexpression.

To determine whether CT20p was directly affecting mitochondrial physiology, we examined cells for changes in the mitochondrial membrane potential ($\Delta\psi\mu$). To this end, we measured the fluorescence emitted by JC-1. The accumulation of JC-1 aggregates in the mitochondrial matrix is dependent on mitochondrial membrane potential, while monomeric JC-1 is cytosolic. Hence, evaluation of JC-1 aggregates to JC-1 monomers reflects the membrane potential of mitochondria. Typically apoptotic activities result in depolarization or low (L) mitochondrial membrane potential. We observed that mitochondria in MDA-MB-231 cells maintained a high (H) to intermediate (I) $\Delta\psi\mu$, which decreased to intermediate (I) levels upon treatment with empty NPs (results from 6 h of treatment shown; Figure 6C). Note that empty NPs did not cause cell death (Figure 3). In contrast, treatment with CT20p-NPs led to cells containing mitochondria with increased or high $\Delta\psi\mu$ (H) (Figure 6C) that did result in eventual cell death (Figure 5B). Hyperpolarization of the mitochondrial membrane is not characteristic of apoptosis but rather could be associated with conditions that cause necrosis.[26] These results collectively suggest that the activity of CT20p, once delivered and released from NPs, triggers a series of intracellular events that may involve mitochondria but result in the eventual rupture of the plasma membrane and cell lysis more consistent with necrotic-like mechanisms.

To demonstrate that CT20p was cytotoxic *in vivo*, a small scale murine tumor experiment was performed. MDA-MB-231 cells were implanted in the flanks of nude mice, and intratumoral or systemic injections of CT20p-NPs peptide were applied once tumors were detected (~9−17 mm^2). Intratumoral injections were performed twice over a period of one week, and significant tumor regression was observed (Figure 7A), as visualized in the representative ultrasound images (Figure 7B). Systemic application of pegylated-CT20p-NPs was achieved with a single intravenous injection, and arrest of tumor growth was also noted (Figures 7A and 7B). Mice were observed daily for two weeks after systemic treatments with CT20p-NPs, and no signs of distress were noted. Upon dissection, tumors in mice that had received injections of CT20p-NPs were undetectable or liquefied, while organs (liver, kidneys, lungs) appeared normal and indistinguishable from control mice. These results are indicative of the potential therapeutic application of CT20p-NPs.

DISCUSSION

Our results revealed that the last 20 amino acid residues of the C-terminus of Bax bear striking similarity to AMPs. Indeed, the presence of cationic and hydrophobic residues, including double lysines, suggests that peptides derived from this C-terminal segment may have the capacity to promote cell death in the absence of an initiating death signal. In addition, the primary sequence of the C-terminal segment of Bax imparts a favorable degree of solubility to CT20p, allowing encapsulation in NPs for delivery to cancer cells. Introduction of CT20p-NPs into colon and breast cancer cells resulted in cell death that is independent of Bax expression and is not suppressed by overexpression of Bcl-2. Unlike the full-length Bax protein, CT20p appears to cause a lethal sequence of events that result in membrane rupture not characteristic of apoptosis. These observations suggest that CT20p has the ability to induce a necrotic-like cell death that is distinct from apoptosis-inducing agents, such as DNA alkylating drugs. Thus, CT20p-NPs could serve as a potent cytotoxic agent for use in combination anticancer regimens together with conventional agents.

Our data suggests that the CT20p may function by forming pores in lipid membranes. This data is bolstered by evidence from a collaborative biophysical study, demonstrating that the structure of CT20p in aqueous solutions was partially α-helical (C-terminus) and partially β-sheet (N-terminus). CT20p could form a pore with a novel structure composed of eight peptide molecules in a strand−turn−helix conformation resulting in an "α/β ring" (Tatulian et al., submitted). Such pores made by CT20p in zwitterionic and anionic lipid membranes caused the release of calcein from loaded lipid vesicles (Garg et al., submitted). In this same study control peptides did not form pores in lipid membranes that caused calcein release, indicating that the observed pore formation was specific to CT20p. Second-order rate kinetics revealed that initial pore formation by CT20p was slow (involving 2−3 peptides), which was followed by a faster rate of assembly involving up to eight peptide molecules. These studies led to a model of an octameric transmembrane pore with an inner diameter of 20−22 Å that could transport calcein, ions or slightly larger molecules (Tatulian et al., submitted). This data coupled with our observation that the CT20p can localize to mitochondria membrane systems in intact cells and cause the release of small molecules from mitochondrial-like lipid vesicles suggests that mitochondria may participate in the necrotic-like cell death we have observed. This implies that CT20p could form pores leading to the release of small ions or molecules sequestered in the mitochondria, consistent with mitochondrial membrane hyperpolarization. These events, in turn, could initiate a lethal cascade of events causing the morphological changes and membrane rupture that we observed in cells treated with CT20p.

A number of studies have focused on harnessing or regulating the activity of Bcl-2 family members to induce the death of cancer cells. The poration activity of α-helical fragments from Bcl-2 proteins has been documented.[27−29] Such studies showed that peptides composed of the α5 and α6 helices of Bax could permeabilize membranes, forming channels that release sequestered contents like calcein,[30,31] providing insights on how the full-length Bax protein may function to

permeabilize mitochondria and induce apoptosis. GFP-tagged versions of the α5 and α6 helices of Bax induced apoptotic cell death as indicated by increased annexin-V binding, PARP cleavage and caspase 3 activation and, when fused to a cell-penetrating motif, caused regression of tumors.[23] In the same study, a GFP-tagged, longer version of the α9 helix of Bax (as compared to CT20p) was tested and did not cause apoptosis.[23] As explanation, the additional residues added to the C-terminal sequence may add rigidity and impair the death-inducing activity we observed with the shorter CT20p. In fact, we previously examined a Bax C-terminal peptide that contained five additional residues (25mer) that was less effective inducing cell death when expressed in cells (data not shown). Other sequences from Bax that have been examined by others include the BH3 domain. In peptide form, the Bax BH3 domain induced apoptosis when used to treat cells.[32] This was mostly due to the BH3 peptide blocking the interaction between Bax and antiapoptotic proteins like Bcl-XL. The Bax BH3 peptide did not directly activate Bax or trigger the translocation of Bax to the mitochondria.[32] This study and others have focused efforts on exploring the indirect use of BH3 peptides as inhibitors of antiapoptotic proteins, such as Bcl-2, rather than as direct activators of cell death via membrane pore formation. The subsequent development and clinical testing of BH3-derived small molecule mimetics[33] is the direct consequence of demonstrating the therapeutic utility of peptides based on functional domains from Bcl-2 proteins.

CT20p shares many of the features of naturally occurring AMPs such as cationic charges (i.e., double C-terminal lysines) and portions of hydrophobic stretches. This may promote selectivity for negatively charged membranes, like those of prokaryotes and also cancer cells. The membranes of cancer cells, because of increased exposure of phosphatidylserine (PS),[34] the presence of sialic acid residues linked to glycoproteins like mucins,[35] and the altered expression of proteoglycans with highly negatively charged side chains,[36,37] tend to accumulate negative charges. Once attracted to membranes, AMPs can kill by necrotic (lysing cell membranes) or apoptotic (disrupting mitochondria) mechanisms. AMPs can also form pores; however, the structural features of these remain to be fully elucidated. A good model from which to compare the action of CT20p is the synthetic peptide, $(KLAKLAK)_2$ (KLA peptide), made to replicate the amphipathic features of AMPs.[38] KLA peptide is poorly permeable to mammalian cells and requires fusion with a cell membrane penetrating agent to enter cells. Most studies report that, once introduced into a cell, the KLA peptide (like CT20p) localizes to mitochondria.[19] Unlike CT20p, however, the KLA peptide causes depolarization of the mitochondrial membrane and apoptosis under most conditions tested.[39,20,40,21] Interestingly, a dose effect was observed when the KLA peptide was fused to prostate cancer antigen in that low doses caused apoptosis, while high doses led to necrosis.[41] We did not observe such effects with CT20p, which caused nonapoptotic cell death with cell lysis at all doses tested, with the major portion of experiments performed in the picomolar range.

In summary, our results suggest that CT20p acts through a nonapoptotic pathway to induce cancer cell death and thereby has potential application with apoptosis-inducing agents in combination therapies to activate multiple death pathways. This is a potent approach to treat cancer in that the targeting of membranes, the rapid mode of action and the necrotic-like death pathway make CT20p an unlikely inducer of cancer drug resistance. We demonstrated herein that CT20p can be encapsulated in polymeric NPs, which increases its bioavailability and enables delivery to tumor cells. We observed tumor regression under both intratumoral and systemic applications, suggesting that CT20p-NPs were accessing the tumor sites through tissue and through the blood. One explanation for this is that the leakiness of the tumor vasculature, the so-called enhanced permeability and retention effect (EPR),[42] helped the CT20p-loaded NPs accumulate within tumors. These results justify the next phase of testing using tumor-targeting nanoparticles for optimal delivery of CT20p in combination treatments to effectively eradicate cancerous cells.

■ ASSOCIATED CONTENT

Ⓢ Supporting Information

Additional experimental details, figures, tables, and movies as discussed in the text. This material is available free of charge via the Internet at http://pubs.acs.org.

■ AUTHOR INFORMATION

Corresponding Author

*Burnett School of Biomedical Sciences, College of Medicine, University of Central Florida, 6900 Lake Nona Blvd, Orlando, FL 32827. Tel: 407-266-7035. Fax: 407-266-7003. E-mail: akhaled@mail.ucf.edu.

Author Contributions

‡Equal contributions.

Notes

The authors declare no competing financial interest.

■ ACKNOWLEDGMENTS

This work was supported in part by NIH/NIGMS Grant GM083324 (A.R.K.) and an ARRA supplement.

■ REFERENCES

(1) Oltersdorf, T.; Elmore, S. W.; Shoemaker, A. R.; Armstrong, R. C.; Augeri, D. J.; Belli, B. A.; Bruncko, M.; Deckwerth, T. L.; Dinges, J.; Hajduk, P. J.; Joseph, M. K.; Kitada, S.; Korsmeyer, S. J.; Kunzer, A. R.; Letai, A.; Li, C.; Mitten, M. J.; Nettesheim, D. G.; Ng, S.; Nimmer, P. M.; O'Connor, J. M.; Oleksijew, A.; Petros, A. M.; Reed, J. C.; Shen, W.; Tahir, S. K.; Thompson, C. B.; Tomaselli, K. J.; Wang, B.; Wendt, M. D.; Zhang, H.; Fesik, S. W.; Rosenberg, S. H. An inhibitor of Bcl-2 family proteins induces regression of solid tumours. *Nature* **2005**, *435*, 677−681.

(2) Oltvai, Z. N.; Milliman, C. L.; Korsmeyer, S. J. Bcl-2 heterodimerizes in vivo with a conserved homolog, Bax, that accelerates programmed cell death. *Cell* **1993**, *74*, 609−619.

(3) Elkholi, R.; Floros, K. V.; Chipuk, J. E. The Role of BH3-Only Proteins in Tumor Cell Development, Signaling, and Treatment. *Genes Cancer* **2011**, *2*, 523−537.

(4) Kroemer, G.; Galluzzi, L.; Brenner, C. Mitochondrial membrane permeabilization in cell death. *Physiol. Rev.* **2007**, *87*, 99−163.

(5) Sturm, I.; Bosanquet, A. G.; Hermann, S.; Guner, D.; Dorken, B.; Daniel, P. T. Mutation of p53 and consecutive selective drug resistance in B-CLL occurs as a consequence of prior DNA-damaging chemotherapy. *Cell Death Differ.* **2003**, *10*, 477−484.

(6) Kuhar, M.; Sen, S.; Singh, N. Role of mitochondria in quercetin-enhanced chemotherapeutic response in human non-small cell lung carcinoma H-520 cells. *Anticancer Res.* **2006**, *26*, 1297−1303.

(7) Castoreno, A. B.; Eggert, U. S. Small molecule probes of cellular pathways and networks. *ACS Chem. Biol.* **2011**, *6*, 86−94.

(8) Pillarisetti, S. Are peptides the future? Small molecule versus peptides. *Curr. Pharm. Biotechnol.* **2006**, *7*, 225−227.

(9) Wilson, W. H.; O'Connor, O. A.; Czuczman, M. S.; LaCasce, A. S.; Gerecitano, J. F.; Leonard, J. P.; Tulpule, A.; Dunleavy, K.; Xiong,

H.; Chiu, Y. L.; Cui, Y.; Busman, T.; Elmore, S. W.; Rosenberg, S. H.; Krivoshik, A. P.; Enschede, S. H.; Humerickhouse, R. A. Navitoclax, a targeted high-affinity inhibitor of BCL-2, in lymphoid malignancies: a phase 1 dose-escalation study of safety, pharmacokinetics, pharmacodynamics, and antitumour activity. *Lancet Oncol.* **2010**, *11*, 1149−1159.

(10) Roberts, A. W.; Seymour, J. F.; Brown, J. R.; Wierda, W. G.; Kipps, T. J.; Khaw, S. L.; Carney, D. A.; He, S. Z.; Huang, D. C.; Xiong, H.; Cui, Y.; Busman, T. A.; McKeegan, E. M.; Krivoshik, A. P.; Enschede, S. H.; Humerickhouse, R. Substantial susceptibility of chronic lymphocytic leukemia to BCL2 inhibition: results of a phase I study of navitoclax in patients with relapsed or refractory disease. *J. Clin. Oncol.* **2012**, *30*, 488−496.

(11) Mason, K. D.; Khaw, S. L.; Rayeroux, K. C.; Chew, E.; Lee, E. F.; Fairlie, W. D.; Grigg, A. P.; Seymour, J. F.; Szer, J.; Huang, D. C.; Roberts, A. W. The BH3 mimetic compound, ABT-737, synergizes with a range of cytotoxic chemotherapy agents in chronic lymphocytic leukemia. *Leukemia* **2009**, *23*, 2034−2041.

(12) Boohaker, R.; Lee, M. W.; Vishnubhotla, P.; Perez, J. M.; Khaled, A. R. The Use of Therapeutics Peptides to Target and to Kill Cancer Cells. *Curr. Med. Chem.* **2012** (Molecular Tools in Cancer Diagnosis and Therapy), in press.

(13) Zhang, L.; Yu, J.; Park, B. H.; Kinzler, K. W.; Vogelstein, B. Role of BAX in the apoptotic response to anticancer agents. *Science* **2000**, *290*, 989−992.

(14) Boohaker, R. J.; Zhang, G.; Carlson, A. L.; Nemec, K. N.; Khaled, A. R. BAX supports the mitochondrial network, promoting bioenergetics in nonapoptotic cells. *Am. J. Physiol.* **2011**, *300*, C1466−C1478.

(15) Santra, S.; Kaittanis, C.; Perez, J. M. Aliphatic hyperbranched polyester: a new building block in the construction of multifunctional nanoparticles and nanocomposites. *Langmuir* **2010**, *26*, 5364−5373.

(16) Hoskin, D. W.; Ramamoorthy, A. Studies on anticancer activities of antimicrobial peptides. *Biochim. Biophys. Acta* **2008**, *1778*, 357−375.

(17) Gray, M. W. The endosymbiont hypothesis revisited. *Int. Rev. Cytol.* **1992**, *141*, 233−357.

(18) Morden, C. W.; Delwiche, C. F.; Kuhsel, M.; Palmer, J. D. Gene phylogenies and the endosymbiotic origin of plastids. *Biosystems* **1992**, *28*, 75−90.

(19) Ellerby, H. M.; Arap, W.; Ellerby, L. M.; Kain, R.; Andrusiak, R.; Rio, G. D.; Krajewski, S.; Lombardo, C. R.; Rao, R.; Ruoslahti, E.; Bredesen, D. E.; Pasqualini, R. Anti-cancer activity of targeted pro-apoptotic peptides. *Nat. Med.* **1999**, *5*, 1032−1038.

(20) Law, B.; Quinti, L.; Choi, Y.; Weissleder, R.; Tung, C. H. A mitochondrial targeted fusion peptide exhibits remarkable cytotoxicity. *Mol. Cancer Ther.* **2006**, *5*, 1944−1949.

(21) Agemy, L.; Friedmann-Morvinski, D.; Kotamraju, V. R.; Roth, L.; Sugahara, K. N.; Girard, O. M.; Mattrey, R. F.; Verma, I. M.; Ruoslahti, E. Targeted nanoparticle enhanced proapoptotic peptide as potential therapy for glioblastoma. *Proc. Natl. Acad. Sci. U.S.A.* **2011**, *108*, 17450−17455.

(22) Walensky, L. D.; Kung, A. L.; Escher, I.; Malia, T. J.; Barbuto, S.; Wright, R. D.; Wagner, G.; Verdine, G. L.; Korsmeyer, S. J. Activation of apoptosis in vivo by a hydrocarbon-stapled BH3 helix. *Science* **2004**, *305*, 1466−1470.

(23) Valero, J. G.; Sancey, L.; Kucharczak, J.; Guillemin, Y.; Gimenez, D.; Prudent, J.; Gillet, G.; Salgado, J.; Coll, J. L.; Aouacheria, A. Bax-derived membrane-active peptides act as potent and direct inducers of apoptosis in cancer cells. *J. Cell Sci.* **2011**, *124*, 556−564.

(24) Li, Y.; Pei, Y.; Zhang, X.; Gu, Z.; Zhou, Z.; Yuan, W.; Zhou, J.; Zhu, J.; Gao, X. PEGylated PLGA nanoparticles as protein carriers: synthesis, preparation and biodistribution in rats. *J. Controlled Release* **2001**, *71*, 203−211.

(25) Alexis, F.; Pridgen, E.; Molnar, L. K.; Farokhzad, O. C. Factors affecting the clearance and biodistribution of polymeric nanoparticles. *Mol. Pharmaceutics* **2008**, *5*, 505−515.

(26) Berghe, T. V.; Vanlangenakker, N.; Parthoens, E.; Deckers, W.; Devos, M.; Festjens, N.; Guerin, C. J.; Brunk, U. T.; Declercq, W.; Vandenabeele, P. Necroptosis, necrosis and secondary necrosis converge on similar cellular disintegration features. *Cell Death Differ.* **2010**, *17*, 922−930.

(27) Basanez, G.; Sharpe, J. C.; Galanis, J.; Brandt, T. B.; Hardwick, J. M.; Zimmerberg, J. Bax-type apoptotic proteins porate pure lipid bilayers through a mechanism sensitive to intrinsic monolayer curvature. *J. Biol. Chem.* **2002**, *277*, 49360−49365.

(28) Garcia-Saez, A. J.; Mingarro, I.; Perez-Paya, E.; Salgado, J. Membrane-insertion fragments of Bcl-xL, Bax, and Bid. *Biochemistry* **2004**, *43*, 10930−10943.

(29) Schlesinger, P. H.; Saito, M. The Bax pore in liposomes, Biophysics. *Cell Death Differ.* **2006**, *13*, 1403−1408.

(30) Garcia-Saez, A. J.; Coraiola, M.; Serra, M. D.; Mingarro, I.; Muller, P.; Salgado, J. Peptides corresponding to helices 5 and 6 of Bax can independently form large lipid pores. *FEBS J.* **2006**, *273*, 971−981.

(31) Garcia-Saez, A. J.; Coraiola, M.; Dalla, S. M.; Mingarro, I.; Menestrina, G.; Salgado, J. Peptides derived from apoptotic Bax and Bid reproduce the poration activity of the parent full-length proteins. *Biophys. J.* **2005**, *88*, 3976−3990.

(32) Moreau, C.; Cartron, P. F.; Hunt, A.; Meflah, K.; Green, D. R.; Evan, G.; Vallette, F. M.; Juin, P. Minimal BH3 peptides promote cell death by antagonizing anti-apoptotic proteins. *J. Biol. Chem.* **2003**, *278*, 19426−19435.

(33) Zhang, L.; Ming, L.; Yu, J. BH3 mimetics to improve cancer therapy; mechanisms and examples. *Drug Resist. Updates* **2007**, *10*, 207−217.

(34) Riedl, S.; Rinner, B.; Asslaber, M.; Schaider, H.; Walzer, S.; Novak, A.; Lohner, K.; Zweytick, D. In search of a novel target - phosphatidylserine exposed by non-apoptotic tumor cells and metastases of malignancies with poor treatment efficacy. *Biochim. Biophys. Acta* **2011**, *1808*, 2638−2645.

(35) Bafna, S.; Kaur, S.; Batra, S. K. Membrane-bound mucins: the mechanistic basis for alterations in the growth and survival of cancer cells. *Oncogene* **2010**, *29*, 2893−2904.

(36) Fadnes, B.; Rekdal, O.; Uhlin-Hansen, L. The anticancer activity of lytic peptides is inhibited by heparan sulfate on the surface of the tumor cells. *BMC Cancer* **2009**, *9*, 183.

(37) viel-Ronen, S.; Lau, S. K.; Pintilie, M.; Lau, D.; Liu, N.; Tsao, M. S.; Jothy, S. Glypican-3 is overexpressed in lung squamous cell carcinoma, but not in adenocarcinoma. *Mod. Pathol.* **2008**, *21*, 817−825.

(38) Javadpour, M. M.; Juban, M. M.; Lo, W. C.; Bishop, S. M.; Alberty, J. B.; Cowell, S. M.; Becker, C. L.; McLaughlin, M. L. De novo antimicrobial peptides with low mammalian cell toxicity. *J. Med. Chem.* **1996**, *39*, 3107−3113.

(39) Mai, J. C.; Mi, Z.; Kim, S. H.; Ng, B.; Robbins, P. D. A proapoptotic peptide for the treatment of solid tumors. *Cancer Res.* **2001**, *61*, 7709−7712.

(40) Kolevzon, N.; Kuflik, U.; Shmuel, M.; Benhamron, S.; Ringel, I.; Yavin, E. Multiple triphenylphosphonium cations as a platform for the delivery of a pro-apoptotic peptide. *Pharm. Res.* **2011**, *28*, 2780−2789.

(41) Rege, K.; Patel, S. J.; Megeed, Z.; Yarmush, M. L. Amphipathic peptide-based fusion peptides and immunoconjugates for the targeted ablation of prostate cancer cells. *Cancer Res.* **2007**, *67*, 6368−6375.

(42) Matsumura, Y.; Maeda, H. A new concept for macromolecular therapeutics in cancer chemotherapy: mechanism of tumoritropic accumulation of proteins and the antitumor agent smancs. *Cancer Res.* **1986**, *46*, 6387−6392.